Effects of magnetic anisotropy on total magnetic field anomalies

Andrea R. Biedermann[1,*], Suzanne A. McEnroe[1,2]

[1] Department of Geology and Mineral Resources Engineering, Norwegian University of Science and Technology, Sem Sælands vei 1, 7491 Trondheim, Norway

[2] Institute for Geoscience and Petroleum, Norwegian University of Science and Technology, Sem Sælands vei 1, 7491 Trondheim, Norway

* Now at: Institute for Rock Magnetism, University of Minnesota – Twin Cities, 116 Church St SE, MN 55455 Minneapolis, USA

Corresponding author: Andrea R. Biedermann (andrea.regina.biedermann@gmail.com)

Key Points:

Magnetic anisotropy affects shape and amplitude of total field anomalies

Neglecting anisotropy causes up to 12° error in interpreted dip for P=1.5, oblate fabric

Estimated mean susceptibility up to -30%/+20% off for P=1.5, oblate fabric

Keywords:

potential field modeling, numerical simulation, magnetic anisotropy, AMS, ARM, fabric, interpretation of magnetic data, remanence-dominated anomaly, layered intrusion

The final version of this manuscript is available from the JGR website

Abstract

Modeling of magnetic anomaly data is a powerful technique to gain information on the shape of subsurface rock bodies. Most models are based on the assumption that the magnetization in the source body is parallel to the direction of the Earth's magnetic field. It has long been recognized that remanent magnetization affects the magnetization direction, intensity and shape of the anomaly, and therefore the interpreted structure. The effects of anisotropy, however, have only received little attention so far. This study uses synthetic models and a case study to investigate how anisotropy affects magnetization and anomalies over a thick dipping sheet, and determines expected errors in interpreted magnetic properties and geometry of the source body for various anisotropy degrees and field inclinations. Anisotropy affects both the shape and amplitude of anomalies. For an oblate uniaxial fabric with the minimum susceptibility normal to the sheet and P = 1.5, errors in interpreted dip are up to 12°, depending on the field inclination, dip, and profile orientation, and errors in estimated mean susceptibility are up to -30%/+20 %, if anisotropy is not taken into account during modeling. These effects are larger for higher degrees of anisotropy. A case study over the MCU IVe' layer in the Bjerkreim Sokndal layered intrusion, Norway, investigates the contributions of (an)isotropic induced and remanent magnetizations to the total field anomalies. There, the influence of anisotropy is mainly related to remanence deflection. The results shown here will help to further improve interpretation of magnetic potential field data.

1. Introduction

Potential field data, e.g. airborne- or ground-magnetic surveys of the magnetic field, provide information about the (magnetic) structure of the subsurface [e.g. *Blakely*, 1996]. Strong magnetization in rocks, induced or remanent, perturbs the local magnetic field and thus generates magnetic anomalies. The amplitude, shape and location of magnetic anomalies depend on (1) size, shape and depth (location) of the source body, (2) induced magnetization, i.e. susceptibility contrast between source body and surroundings, (3) the contribution of natural remanent magnetization (NRM), and (4) the intensity and orientation of the local geomagnetic, i.e. inducing, field, which varies with latitude. Models of how source geometry, location, and inducing field direction influence anomalies are readily available for simple bodies uniformly magnetized in the direction of the inducing field [e.g. *Blakely*, 1996; *Smellie*, 1956]. These models are based on two assumptions: the magnetization is parallel to the inducing field, and the anomaly is small enough that the anomalous component of the field is parallel to the Earth's field [e.g. *Zietz and Henderson*, 1956].

It has been long recognized that the total magnetization of a source body is not necessarily parallel to the inducing field, e.g. due to magnetic remanence [*Sutton and Mumme*, 1957]. *Hall* [1959] reported that it is important to model magnetic anomalies based on the total magnetization, i.e. the sum of induced and remanent magnetizations, and derived equations to compute the magnetic field of bodies with arbitrary magnetization direction. *Arkani-Hamed and Celetti* [1989] investigated the influence of thermal remanent magnetization on anomalies above igneous intrusions of various sizes and emplacement depths. A number of methods have been developed to determine the total magnetization (or the direction and intensity of the remanent contribution to the magnetization), either directly by measuring magnetic properties, or indirectly from aeromagnetic survey data [*Clark*, 2014]. It is also known that, for strongly magnetic rocks, effects of self-demagnetization have to be taken into account, as they may influence both the intensity and direction of magnetization [*Clark and Emerson*, 1999; *Emerson et al.*, 1985; *Guo et al.*, 2001]. These can be modelled accurately for an ellipsoid [*Osborn*, 1945], and can be approximated for other shapes [*Chen et al.*, 1991; *Sato and Ishii*, 1989]. Due to the non-uniqueness of potential field models, several source bodies with different geometries and magnetic properties can result in similar anomalies. In particular, neglecting the effects of remanence can lead to severe misinterpretations concerning the location or dip of a source body [*Clark*, 1997; 2014].

Another mechanism that affects the direction and intensity of magnetization in a source body is magnetic anisotropy. To date, only few studies have discussed the effects of magnetic anisotropy on total field anomalies [*Clark*, 1997; *Clark and Schmidt*, 1994; *Emerson et al.*, 1985; *Florio et al.*, 1993], even though it has been shown that these effects can be significant: *Clark and Schmidt* [1994] investigated magnetic anomalies related to banded iron formations (BIFs) in Western Australia, and state that *"an interpretation of the magnetic signatures that ignores anisotropy and remanence will lead to serious errors, particularly in interpreted dips. For a given anisotropy, the error in interpreted dip depends on the angle between the inducing field and the bedding plane. Assuming remanence is negligible, there is no deflection of induced magnetization and hence no dip error, when the field is either parallel to or normal to bedding."*

Magnetic anisotropy can affect anomalies in two ways: (1) directly, by deflecting the induced magnetization away from the geomagnetic field and towards the maximum principal susceptibility axis, and (2) indirectly, through the effects it has on the direction and intensity of a remanent magnetization. The former process is controlled by anisotropy of susceptibility and dominated by high-susceptibility minerals, whereas the latter is controlled by the anisotropy of the remanence-carrying fraction. Depending on rock type and mineralogy, the anisotropy of magnetic susceptibility (AMS) and anisotropy of remanent magnetization can be related to the same mineral (e.g. magnetite), or to different ferromagnetic minerals (e.g. magnetite, hematite, and hemo-ilmenite). In some rocks, paramagnetic minerals can carry the AMS, which may have a minor effect on the induced anomaly. Even though the underlying physical processes are different, the effects of both AMS and remanence anisotropy on magnetization direction and intensity can be described in the same way mathematically.

This study consists of a synthetic part, using numerical models to investigate the general effects of anisotropy, and a case study, applying the results from the synthetic models to a specific geological area in the Bjerkreim Sokndal (BKS) layered intrusion, Southern Norway. The synthetic part of the study characterizes (1) how magnetic anisotropy influences the magnetization of a dipping sheet whose minimum susceptibility is normal to the sheet for different dips of the sheet, and inclinations of the inducing field, (2) how total field anomalies measured above this sheet compare to anomalies of an isotropic sheet of the same size and orientation, and (3) what error is made when the anomaly above an anisotropic sheet is interpreted as if the magnetic properties of the source body had been isotropic. Input parameters (source geometry and magnetic anisotropy) for the synthetic models reflect the properties of the case study area, but are applicable to any region with similar source geometry and anisotropy parameters, independent of rock type or mineralogy. Moreover, synthetic models are calculated for various field inclinations, making it possible to determine anisotropy effects for a range of latitudes. The case study is performed over 5 profiles across the MCU IVe' layer of the BKS intrusion. The BKS exhibits both prominent anomalies and well defined mineral fabrics and associated magnetic anisotropy. We will use magnetic properties of surface samples (susceptibility, anisotropy of susceptibility and magnetic remanence), as well as geometrical information from previous studies to create forward models of induced, anisotropic, remanent and total magnetic anomalies. These models can be used to determine the effects of each contribution, and are compared to ground magnetic data measured along several profiles.

2. Synthetic models

2.1 Model setup

The models reflect a dipping layer and can be applied to any geological setting of similar geometry, e.g. a layer in a layered intrusion. The layer geometry was approximated by a thick dipping sheet of infinite extension along strike and semi-infinite in depth (Figure 1). Layer thickness is 200 m, and the depth to the top of the layer was set to 2 m, corresponding to the approximate height of the magnetometer above ground in our ground-magnetic survey. Profiles were oriented S-N, SW-NE, and W-E (i.e. 0°, 45° and 90°, respectively) and the strike of the dipping sheet is always normal to the profile orientation (-90°, -45° and 0°).

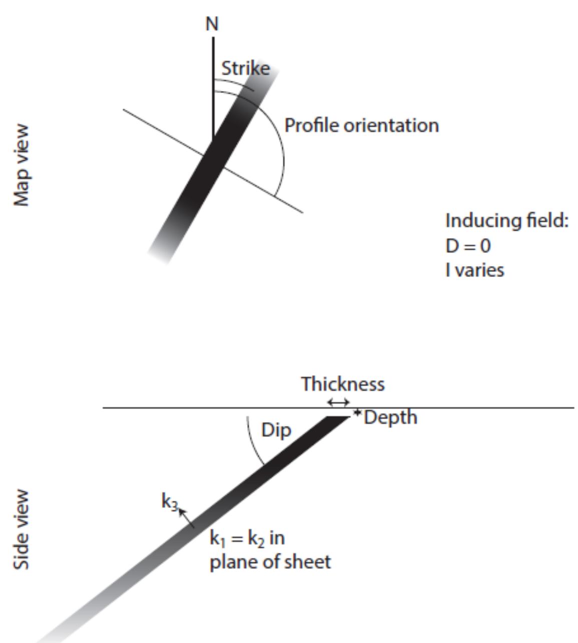

Figure 1: Synthetic model setup. Thickness = 200 m, depth = 2 m, profile orientation = 0° (S-N), 45° (SW-NE) or 90° (W-E), perpendicular to the strike of the sheet. The dip of the sheet varies from 0 to 180°. Magnetic field declination is set to 0°, and inclination varies from 0 to 90°. The magnetic fabric is oblate and linked to the dip of the sheet, with k_3 always normal to the sheet, and P equals 1.2 or 1.5.

Total field anomalies were calculated in MatLab using the equations given by *Hall* [1959]. The model computes the projection of the anomalous field vector onto the vector of the inducing geomagnetic field. Therefore, results of these synthetic models are valid as long as the anomaly is small compared to the regional inducing field. Very strong anomalies (e.g. due to large susceptibilities) will distort the geomagnetic field, which would have to be taken into account during modeling. Hence, results presented here for synthetic models are independent of mean susceptibility, provided that the susceptibility is small enough so that the anomalies do not distort the inducing field. Anisotropy and self-demagnetization have been incorporated in the models following the procedure outlined in *Emerson et al.* [1985]. In general, the magnetization in a rock consists of two components, Induced and remanent. Magnetic anisotropy can affect the intensity and direction of both of these components: induced magnetization, $\vec{M}_{ind} = k\vec{H}$, is not parallel to the inducing field $\vec{H}$, unless the susceptibility tensor *k* is isotropic, or $\vec{H}$ is parallel to one of the eigenvectors of *k.* Additionally, for an anisotropic *k*, the strength of $\vec{M}_{ind}$ will vary with the orientation of $\vec{H}$. The induced magnetization and related potential field anomaly are affected by all minerals in a rock, but often dominated by magnetite and its shape and/or distribution anisotropy.

Anisotropy effects on remanent magnetization can be described by $\vec{M}_{rem} = k_{rem}\vec{H}$, where $\vec{H}$ is the field at the time of remanence acquisition, and k_{rem} the remanence susceptibility tensor. If the rock possesses remanence anisotropy, the NRM will be deflected away from the field in which it was acquired, and its intensity depends on the orientation of the remanence fabric with respect to that field, similar to the effects AMS has on the induced magnetization. The remanent magnetization and its anomaly are only affected by the remanence-carrying minerals. Thus, whereas the two tensors *k* and k_{rem} can be coaxial if they are dominantly carried by the same mineral, in multiphase systems when they are carried by different minerals, *k* and k_{rem} can have different orientations resulting in different effects on magnetization deflection and anomalies. Additionally, the field vectors can be different due to secular variation or tectonic movements after remanence acquisition. Nevertheless, both processes are described by the same type of equation, $\vec{M} = k\vec{H}$, which will be investigated here based on the example of induced magnetization and its anomalies.

These synthetic models will serve to characterize how magnetic anisotropy can affect the magnetization vector and shape and intensity of magnetic anomalies. Because only the direction and intensity of magnetization in a rock, but not the nature of magnetization, induced or remanent, are important to compute anomalies, the general findings regarding the effects of magnetization deflection and anomalies can be adapted for remanent magnetization. The tensor *k* can be described by its eigenvalues or principal susceptibilities $k_1>=k_2>=k_3$, and the corresponding eigenvectors, i.e. the principal susceptibility directions (characterized by their declination D_i and inclination I_i, $i = 1, 2, 3$). The degree of anisotropy is quantified by $P = k_1/k_3$, and the shape by $U = (2k_2 - k_1 - k_3)/(k_1 - k_3)$, where U = 1 represents oblate shapes [*Hrouda*, 1982; *Jelinek*, 1981]. For the purpose of this study, the magnetization intensity obtained from the tensor calculation $\vec{M} = k\vec{H}$ will be normalized by the corresponding isotropic or scalar $M = k_{mean}H$, where $k_{mean} = (k_1+k_2+k_3)/3$. For the self-demagnetization correction, N = 0 was used in directions within the dipping sheet, and N = 1 in the direction normal to the sheet, in accordance with self-demagnetization factors for BIFs of similar geometry [*Clark and Schmidt*, 1994].

This code was used to investigate under which circumstances the effects of anisotropy are strongest. Models were run using various profile orientations, dips of the thick dipping sheet, and degrees of anisotropy. The magnetic fabric orientation was approximated by an oblate shape, U=1 and k_1=k_2, with the minimum susceptibility normal to the dipping sheet, i.e. the orientation of the magnetic fabric is linked to the dip of the sheet.

2.2 Influence of magnetic fabric on direction and intensity of induced magnetization

Figure 2 shows how the inclination of $\vec{M}_{ind}$ changes as a function of the dip of the sheet (and thus magnetic fabric) for different inclinations of the inducing field, and two profile orientations, S-N (profile orientation = 0°) and W-E (profile orientation = 90°). On a S-N-profile, the deflection of $\vec{M}_{ind}$ away from the direction of $\vec{H}$ depends on the degree of anisotropy, and equals a maximum of ±5^{o} for P = 1.2 and a maximum of ±12^{o} for P = 1.5. No deflection is observed when one of the principal susceptibility axes is parallel to the inducing field, i.e. when the dip of the sheet is 90^{o}-I or 180^{o}-I, where I is the field inclination.

For a W-E profile, the magnetization will always be flatter than the inclination of the inducing field, except when the dip of the sheet is exactly vertical, or for a field inclination of 0^{o}. In these cases, no deflection is observed. The maximum deflection corresponds to -5^{o} and -12^{o} for P = 1.2 and 1.5, respectively, and occurs for a field inclination of 50^{o} and shallow dips of the sheet.

The intensity of $\vec{M}_{ind}$ is also affected by the magnetic fabric (Figure 2). It ranges between k_3/k_{mean} to k_1/k_{mean} times the magnetization expected for an isotropic body with the same mean susceptibility, and reaches a maximum when $\vec{H}$ lies within the plane of the dipping sheet (i.e. the k_1=k_2-plane). Likewise, the magnetization is minimum when $\vec{H}$ is normal to the sheet (i.e. parallel to k_3).

2.3 Influence of magnetic fabric on the intensity and shape of induced total field anomalies

The amplitude and the shape of a total field anomaly differ when the source body is a thick dipping sheet with anisotropic k (cf. Figure 1), compared to the anomaly over the same sheet with isotropic k equal to k_{mean}. Note that no anomalies are produced for perfectly horizontal infinite sheets, which is why all results are given for dips ranging from 1 to 179°. The amplitude of the total field anomaly will be defined as the difference between its maximum and minimum value. In order to compare the intensity of anomalies for the isotropic and anisotropic case, the quantity $ADiff = \frac{Amplitude_{Anisotropic} - Amplitude_{Isotropic}}{Amplitude_{Isotropic}} * 100$ (%) was defined (Figure 3).

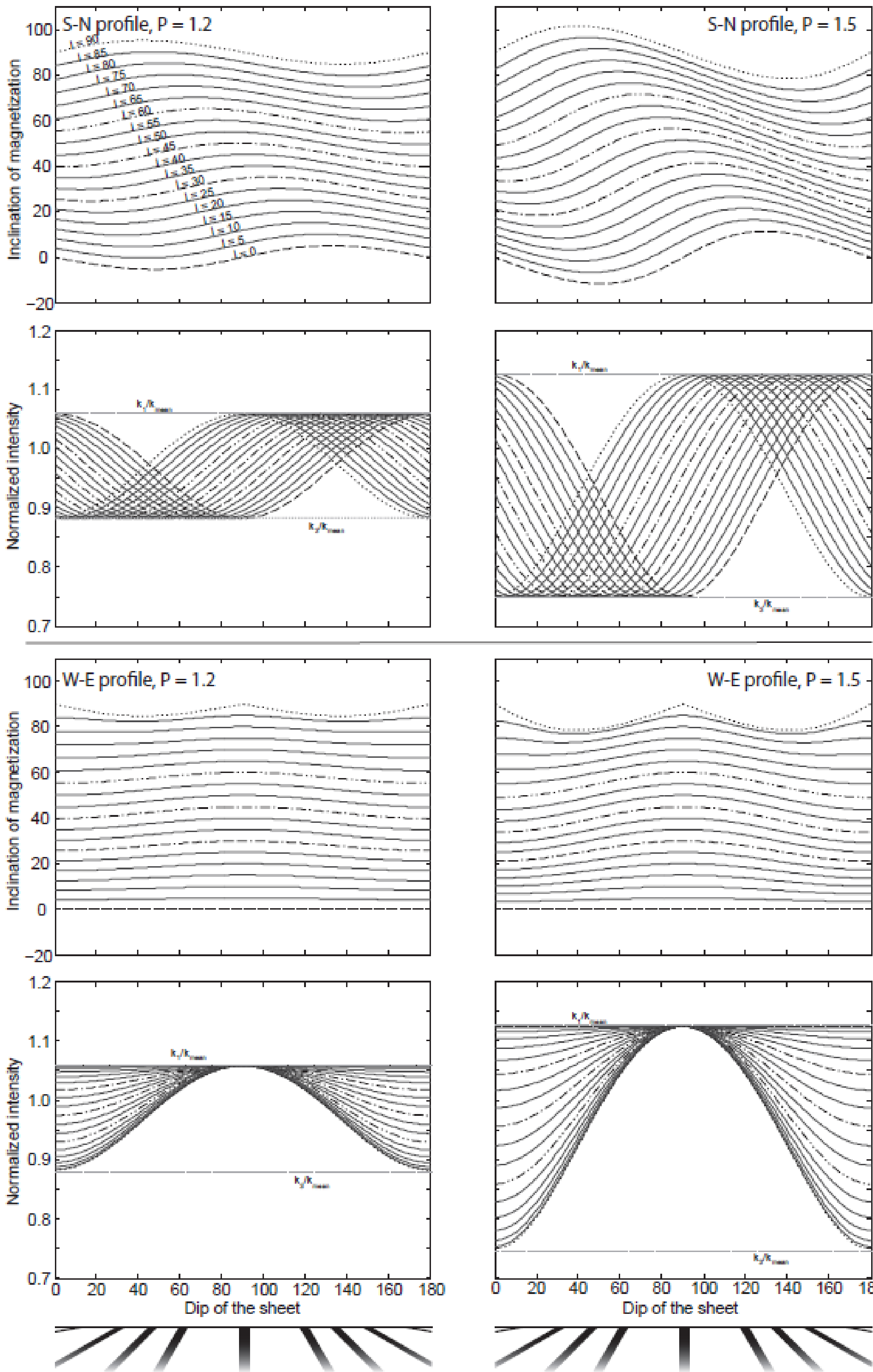

Figure 2: Effect of magnetic anisotropy on the direction and intensity of magnetization for P = 1.2 and P = 1.5, and a S-N and a W-E profile. Field inclination 0:5:90, dip 0:1:180. Grey solid lines show results for inclinations in 5° intervals. Inclinations of 0°, 30°, 45°, 60°, and 90° are highlighted in black, and using different line styles: - - (0°), - - . - -. (30°), - . - . (45°), - . . - . . (60°), and . . (90°), in this and subsequent figures.

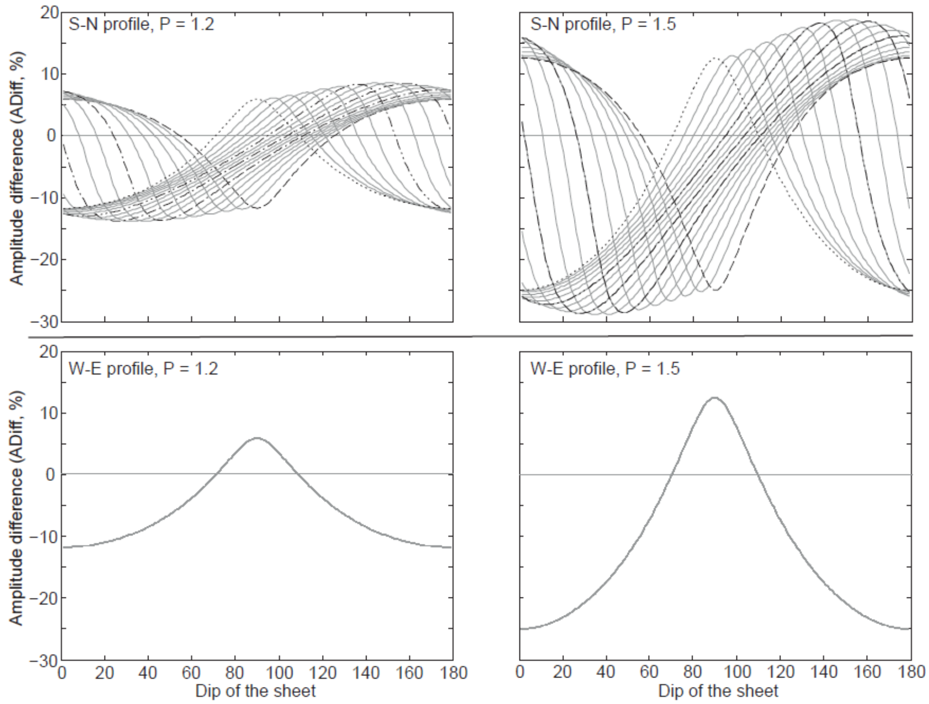

Figure 3: Effect of anisotropy on the amplitude of observed total field anomalies for P = 1.2 and P = 1.5, and a S-N and W-E profile.

Like the effects of anisotropy on the magnetization vector, the effect of anisotropy on the anomaly amplitude is larger for higher degrees of anisotropy. For a S-N-profile and if the inducing field is vertical (I = 90^o), the amplitude of the anomaly increases by k_1/k_{mean} when the sheet dips vertically, and k_1 is parallel to $\vec{H}$, and approaches a decrease by k_3/k_{mean} when the sheet is nearly horizontal, so that the k_3 direction is close to $\vec{H}$. The opposite is true when $\vec{H}$ is horizontal (I = 0^o): the anomaly amplitude is decreased for a vertically dipping sheet, and increases for shallowly dipping sheets. In these special cases, the change in anomaly amplitude is merely due to changes in the intensity of the magnetization, and $\vec{M}_{ind}$ is parallel to $\vec{H}$. In the more general case (i.e. when $\vec{H}$ and $\vec{M}_{ind}$ are not parallel to the principal susceptibility axes), both the anisotropy-related change in magnetization intensity, and also the deflection of $\vec{M}_{ind}$ away from $\vec{H}$ affect the observed anomaly. Therefore, the influence of anisotropy on the amplitude of the anomaly appears largest for field inclinations between 40 and 50°, both for P = 1.2 and P = 1.5. The amplitude of the measured anomaly is a complex function of (1) the orientation of the inducing field (= measurement direction) with respect to the magnetic fabric, (2) the orientation of the magnetization with respect to the fabric, and (3) the angle between the inducing field and the magnetization. Therefore, no simple relationship such as 'the effect of anisotropy is largest if the field is parallel to the maximum or minimum susceptibility', or 'the effect of anisotropy is largest if the magnetization is parallel to the maximum or minimum susceptibility' can be established. Because the synthetic models rely solely on source geometry and the orientation, shape and degree of the magnetic fabric, these findings can be applied to any source body with similar anisotropy, independent of rock type, mineralogy, or whether the magnetic fabric is an AMS or remanence anisotropy.

For a W-E profile, the influence of the anisotropy is independent of field inclination, as long as $I > 0^o$. It resembles that of $I = 90$ in a S-N-profile. This is because only the vertical component of the magnetization will cause an anomaly, while the horizontal component, which is oriented S-N and thus is along-strike, does not contribute. No anomaly is generated if $I = 0^o$, because in this special case, all the magnetization is along-strike, both in the isotropic and anisotropic scenarios.

As magnetic anisotropy affects the direction of the magnetization, it will also influence the shape of the anomalies, unless $\vec{H}$ is parallel to one of the principal susceptibility axes (Figure 4a). In terms of the magnetization direction, one can differ between two cases, depending on the dip of the sheet, i.e. the orientation of the magnetic fabric: (1) anisotropy causes $\vec{M}_{ind}$ to be steeper than $\vec{H}$, and (2) anisotropy leads to an induced magnetization shallower than $\vec{H}$. However, this cannot be directly translated to interpreted dips being too steep or too shallow, as they also depend on the inclination of $\vec{H}$. For example, if $\vec{H}$ is vertical ($I = 90^o$), anisotropy will cause $\vec{M}_{ind}$ to be more shallow, except when the dip of the sheet equals 90^o, where $\vec{M}_{ind}$ is parallel to $\vec{H}$. If the sheet has a dip angle different from 90^o, the anomaly created by an anisotropic sheet will have the same shape as that generated by an isotropic sheet dipping more steeply (Figure 4b). The error in interpreted dip when anisotropy is neglected depends on the orientation of the sheet with respect to $\vec{H}$, and is up 12^o for $P = 1.5$ (Table S1, Supplementary Information). If $\vec{H}$ is horizontal ($I = 0^o$), $\vec{M}_{ind}$ will point slightly upwards for dips $<90^o$, be parallel to $\vec{H}$ for dip = 90^o, and point slightly downwards for dips $>90^o$ (for consistency, we will use dip angles 0-180^o as defined in Figure 1 throughout this paper, instead of N-dipping and S-dipping angles between 0-90^o). In this case, and measured along a S-N profile, the interpreted dip will be too shallow if anisotropy is neglected. The error again varies with the dip of the sheet. If $\vec{H}$ has an inclination of 45^o, the anisotropic anomaly appears like the isotropic anomaly of a more shallowly dipping sheet if dip < 45^o, and that of a more steeply dipping isotropic anomaly if dip > 135^o. For 45^o < dip < 135^o, the anomalies look the same for the anisotropic sheet, as for an isotropic sheet having a larger dip angle. If anisotropy is neglected, this leads to too steep interpreted dips for dip < 80^o, to misinterpretation concerning N-dipping vs S-dipping structures when the sheet is nearly vertical, to too shallow interpreted dips if dip > 90^o. Similar observations are made for other intermediate field inclinations.

In the case of W-E profiles, and $I = 0^o$, no anomalies are observed. For $I > 0^o$, only the vertical component of the field creates an anomaly, and the interpreted isotropic dip is up to 12^o steeper than the true dip of the anisotropic structure for $P = 1.5$.

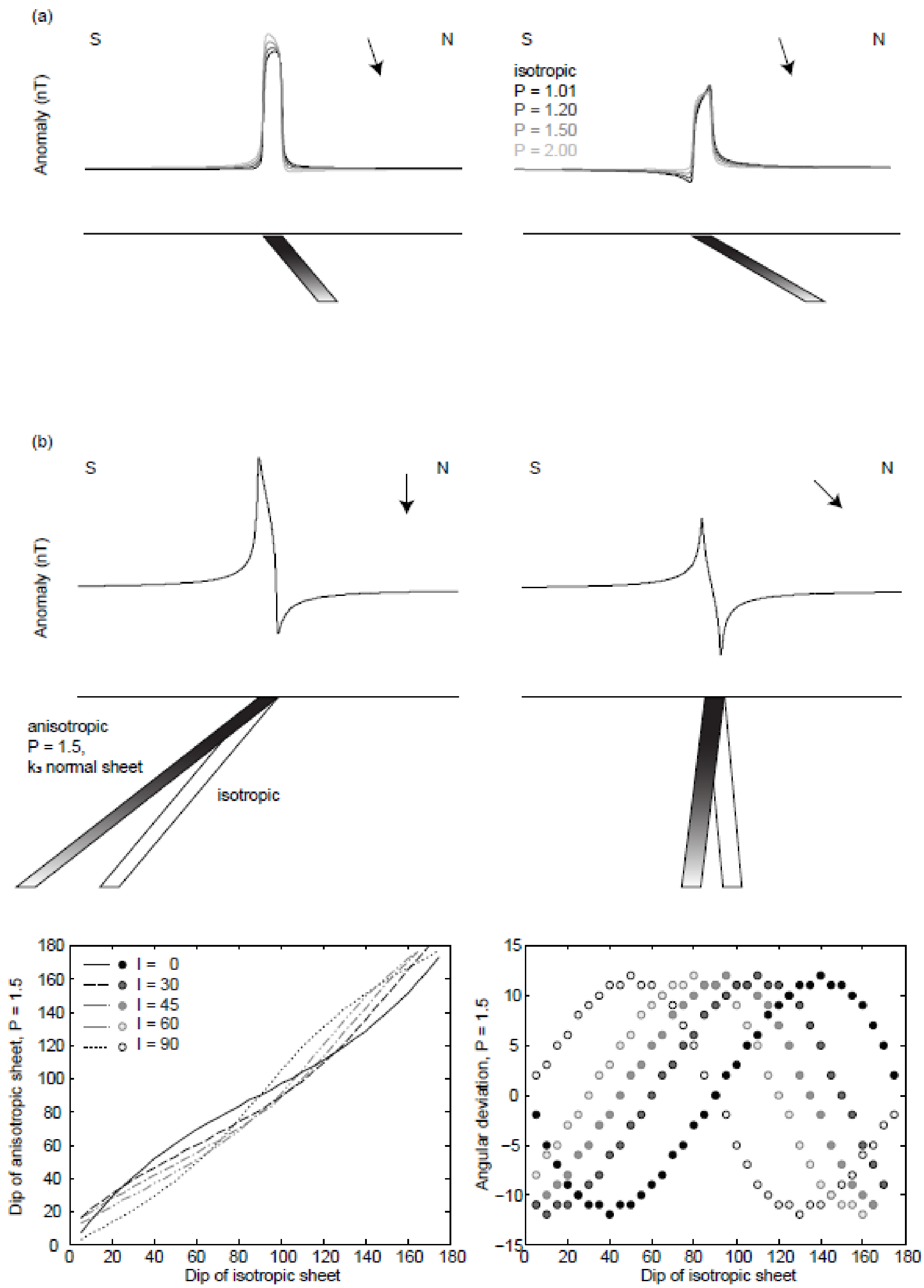

Figure 4: (a) Comparison of different anomaly shapes for the same geometry, but different degrees of anisotropy; (b) Comparison of isotropic and anisotropic anomalies, P = 1.5. (top) Examples of different dips for isotropic and anisotropic models resulting in the same anomaly shape. (bottom) Dip of anisotropic sheet as a function of the dip of isotropic sheet for the same shape of the anomaly, and difference between the isotropic and anisotropic dip as a function of isotropic dip. Resolution 1°

3. Bjerkreim Sokndal (BKS) case study

3.1 Geological setting

The study area is the Proterozoic BKS layered intrusion in Rogaland, Southern Norway [*Robins and Wilson*, 2001; *Wilson et al.*, 1996]. It covers 230 km^2 and is made up of plagioclase-pyroxene oxide cumulates, overlain by acidic rocks. The cumulate series consists of several megacyclic units (MCU), representing magma recharge and fractional crystallization [*Duchesne*, 2001; *Duchesne and Charlier*, 2005; *Wilson et al.*, 1996]. Two iron oxides, magnetite and hemo-ilmenite occur in varying amounts in the intrusion, and changes in oxide mineralogy generate a sequence of positive and negative magnetic anomalies, i.e. above and below background levels [*McEnroe et al.*, 2009; *McEnroe et al.*, 2001]. Strong magnetic contrasts have been reported: 6,000 nT in a fixed wing aeromagnetic survey at 150 m elevation, or nearly 16,000 nT, with intensities varying from 38,649 nT to 54,243 nT in a helicopter survey 45 m above ground [*McEnroe et al.*, 2001]. A negative anomaly of -13,000 nT (helicopter survey) has been related to one layer of the intrusion, MCU IVe', close to Heskestad (McEnroe et al., 2004b). The MCU IVe' layer has been defined based on its strong remanence and high ratio of remanent to induced magnetization [*McEnroe et al.*, 2009]. Existing ground magnetic surveys report an anomaly of -27,000 nT, being most intense where the cumulate layering is nearly vertical in Heskestad [*McEnroe et al.*, 2004a], and -30,900 nT also in Heskestad [*McEnroe et al.*, 2004b]. This anomaly is dominated by remanent magnetization, and a remanence intensity of 24 A/m is needed to model the magnetic data [*McEnroe et al.*, 2004b].

The entire intrusion underwent solid-state deformation and today forms a syncline, whose base has been estimated to 4 – 9 km depth [*Bolle et al.*, 2002; *Deemer and Hurich*, 1997; *Paludan et al.*, 1994; *Smithson and Ramberg*, 1979]. Two types of structural elements have been described: (1) the original igneous layering, and (2) foliation, which is parallel to the layering on the limbs of the syncline, and parallel to the fold axial surface in the hinge zone [*Paludan et al.*, 1994]. The preferred mineral alignment and distribution of minerals related to these structures gives rise to magnetic anisotropy, both in the cumulate series and the overlying acidic rocks [*Biedermann et al.*, 2016; *Bolle et al.*, 2000]. *Biedermann et al.* [2016] report strong anisotropy of magnetic susceptibility (AMS) and anhysteretic remanence (AARM), with *P*-values up to 2.71 (AMS) and 3.62 (AARM) in the MCU IVe' layer of the BKS. The orientation of the magnetic fabric changes for different locations along the layer, and in general, the minimum susceptibility is normal to the layering or foliation.

Magnetic properties of rocks throughout the BKS intrusion vary significantly, with site mean susceptibilities ranging from $0.16*10^{-2}$ to $17.9*10^{-2}$ (SI) and site mean NRM ranging from 0.15 to 52 A/m, with layer-averaged NRMs of 3.6 A/m, 19 A/m and 2 A/m for layers MCU IVd, MCU IVe' and MCU IVf, respectively [*McEnroe et al.*, 2009]. *McEnroe et al.* [2004a] report average susceptibilities of $8*10^{-2}$, and an average NRM of 30.6 A/m for the MCU IVe layer, with NRM intensities up to 74 A/m. The intensity of the NRM is strongest in the Heskestad area [*Brown and McEnroe*, 2015; *McEnroe et al.*, 2004a; 2009; *McEnroe et al.*, 2001]. Other than changes in mineralogy or cooling history, i.e. the concentration and composition of remanence carriers and the number/generations of hemo-ilmenite exsolution lamellae that developed, also magnetic anisotropy may influence the intensity and direction of NRM and hence the strength and shape of the anomaly. Based on lamellar magnetism theory, *McEnroe et al.* [2004b] state that '*if (001) planes of ilmenite are oriented parallel to the magnetizing field at lamellar separation and further if a-crystallographic axes are also parallel to the field, lamellae will form magnetically 'in phase', with resulting very strong magnetic moment. At Heskestad the steep foliation and lineation are both quasi-parallel to the early Neo-Proterozoic magnetizing field, fulfilling these requirements […]'* to explain the strong NRM in this area. *Robinson et al.* [2013] investigated NRM and preferred orientation of hemo-ilmenite in Allard Lake, Canada, and show a strong dependence of NRM intensity on the orientation of hematite-ilmenite lamellae with respect to the magnetizing field. *Biedermann et al.* [2017] observed that the NRM orientation changes along the MCU IVe' layer, and appears to be tilted towards the direction of k_1.

3.2 Sample description and magnetic properties

Surface samples have been collected from various locations in the MCU IVe' layer, and additional samples from the MCU IVe' layer and other layers of the intrusion were available from previous studies (Figure 5). A detailed description of sampling and sample preparation is given in *Brown and McEnroe* [2015] and *Biedermann et al.* [2016]. Throughout this study, magnetic property results will be shown for two sets of samples: in total, 570 samples from 101 sites have been used, including samples from layers IAa, IBa, IBc, IBe, IIc, IIIa, IIIc, IIId, IIIe, IIIf, IVa, IVb, IVc, IVd, IVe, IVe', IVf, and mangerite, and 310 of these from 39 sites originate within the MCU IVe' layer.

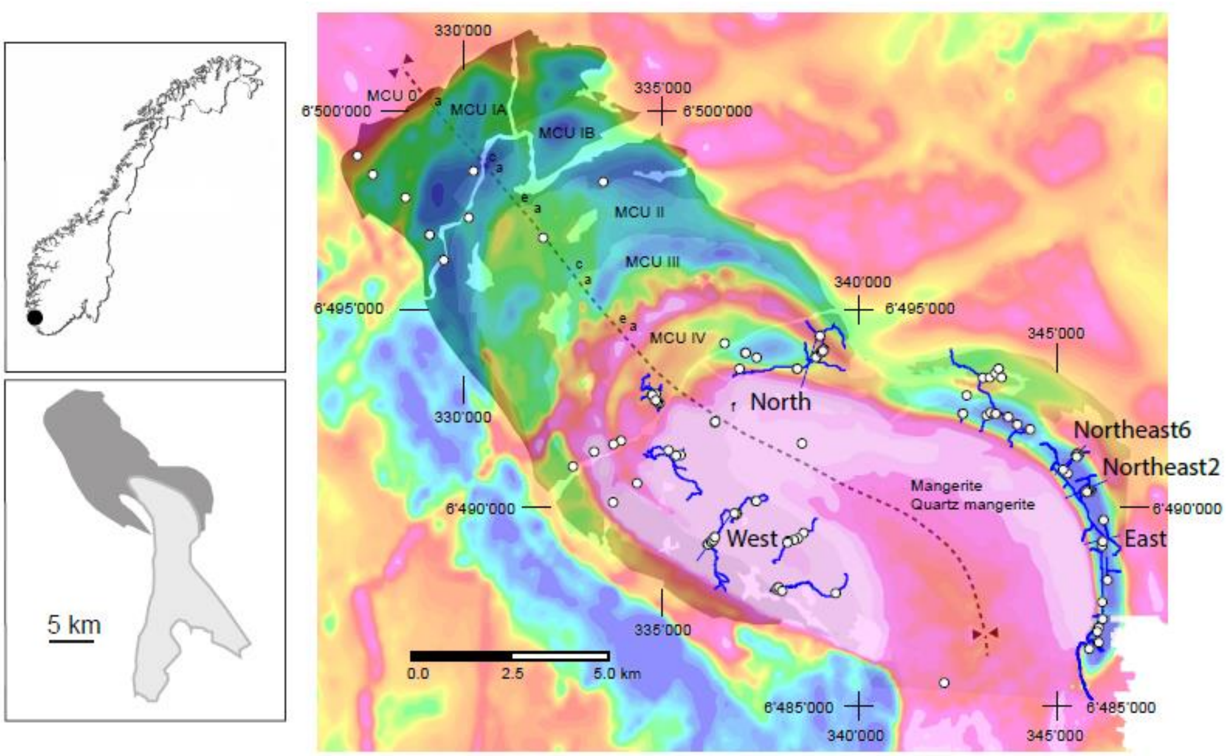

Figure 5: Simplified map of the BKS intrusion including sample locations and ground magnetic and projected profiles; coordinate system UTM32N. Overlain by aeromagnetic data from NGU.

Magnetic properties that were measured include (1) AMS, including mean susceptibility (570 samples) and (2) intensity and direction of NRM (464 samples). AMS of part of the samples has been described by *Biedermann et al.* [2016], and additional samples were measured using the same procedure. Magnetic susceptibility will be described by k_{mean} as determined from AMS measurements, which is more accurate than a single bulk susceptibility measurement. AMS was determined in a field of 200 A/m, which is higher than the geomagnetic field (ca. 40 A/m). Because some minerals, e.g. pyrrhotite [*Martin-Hernandez et al.*, 2008; *Worm* 1991; *Worm et al.,* 1993] or hematite [*Guerrero-Suarez and Martin-Hernandez*, 2012] have been reported to display field-dependence of susceptibility and AMS, test measurements were made on a subset of samples in 5 A/m, 40 A/m, and 200 A/m. These showed no field-dependence on either mean susceptibility, principal susceptibility directions, AMS degree, or AMS shape. Both the susceptibility and the AMS of the MCU IVe' rocks are dominated by multi-domain magnetite grains. AMS is described by the same tensor properties like for the synthetic models. Note that because the susceptibility in these samples is strong, all measured values had to be corrected for the effects of self-demagnetization, using the equation $k_{intrinsic} = k_{measured}/(1 - N * k_{measured})$ [e.g. *Clark*, 2014]. The self-demagnetization tensor *N* only has an exact analytical solution for ellipsoids with homogeneous properties. Paleomagnetic samples have a height/diameter ratio of 0.88, as close as possible to a spherical sample [*Porath et al.*, 1966], and N can be approximated to be isotropic and equals 1/3. Throughout the BKS intrusion, mean susceptibility varies over several orders of magnitude, from $5*10^{-4}$ to 0.23 (SI). Within the MCU IVe' layer, the site mean magnetic susceptibility ranges from 0.01 to 0.22, with a typical k_{mean} around 0.1, in agreement with previous studies (Figure 6). All samples show significant AMS, with *P*-values up to 3.6 for all samples, and up to 2.7 for the MCU IVe' layer [cf. *Biedermann et al.*, 2016]. An AMS degree *P* slightly below 1.5 is typical, both throughout the intrusion and in the MCU IVe' layer.

NRM intensity and direction, as well as stability of NRM during demagnetization has been described previously, and additional samples were measured by the same methods [*Biedermann et al.*, 2017; *Brown and McEnroe*, 2015]. Mean NRMs were calculated as vector averages, i.e. by adding all the (un-normalized) vectors together and dividing by the number of samples [*Clark*, 2014]. As for susceptibility, because the observed magnetizations are strong, corrections for self-demagnetization were necessary: $NRM_{intrinsic} = (1 + k_{intrinsic} * N) * NRM_{measured}$, where N = 1/3 for paleomagnetic cores [*Clark*, 2014]. Intrinsic NRM intensities vary from 0.03 A/m to 61.7 A/m throughout the entire sample collection, and from 0.7 A/m to 61.7 A/m in the MCU IVe' layer. Newly measured NRMs have been corrected for self-demagnetization effects with the NRM and mean magnetic susceptibility of each sample.

Koenigsberger ratios, $Q = {}^{M_{rem}}/_{M_{ind}}$ were calculated by assuming an inducing field *H* of 50'650 nT (http://www.ngdc.noaa.gov/geomag-web/?model=igrf, average field in field area in May 2015 when the fieldwork was carried out). Intrinsic NRM and induced magnetization were used to compute Koenigsberger ratios. If Q >> 1, the remanent magnetization dominates over the induced magnetization, whereas Q << 1 means that the remanence can be neglected in the modeling.

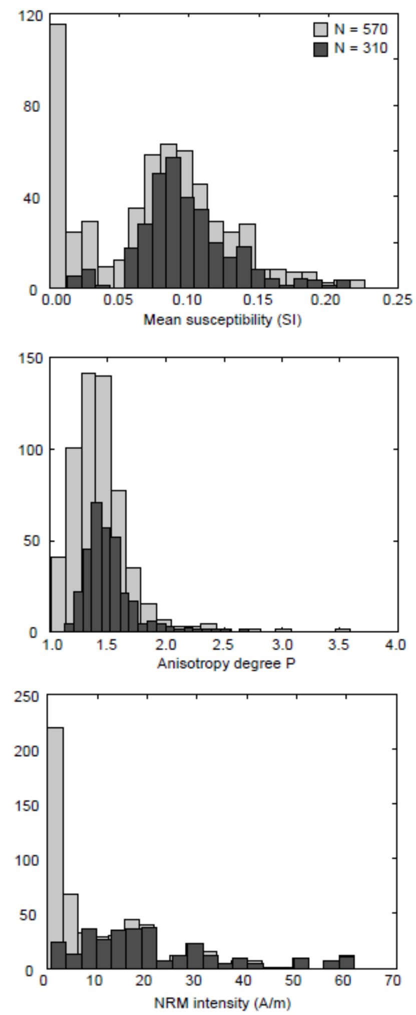

Figure 6: Histogram of kmean, P-value, and NRM intensity (light grey: complete set of samples throughout intrusion, dark grey: subset, MCU IVe' layer)

Koenigsberger ratios range between 0.1 and 50 over all samples, and from 0.3 to 50 in the MCU IVe' layer. The majority of Koenigsberger ratios outside this layer are lower than within the layer,, consistent with results shown by *Brown and McEnroe* [2015]. Figure 7 shows a plot of induced vs remanent magnetization and the variation in Q-values. The high Q-values indicate that remanence contributes significantly to the total field anomalies in this area. Variations in Q reflect variations in oxide-rich layers (dominated by magnetite vs hemo-ilmenite) related to magma recharge events [*McEnroe et al.*, 2009].

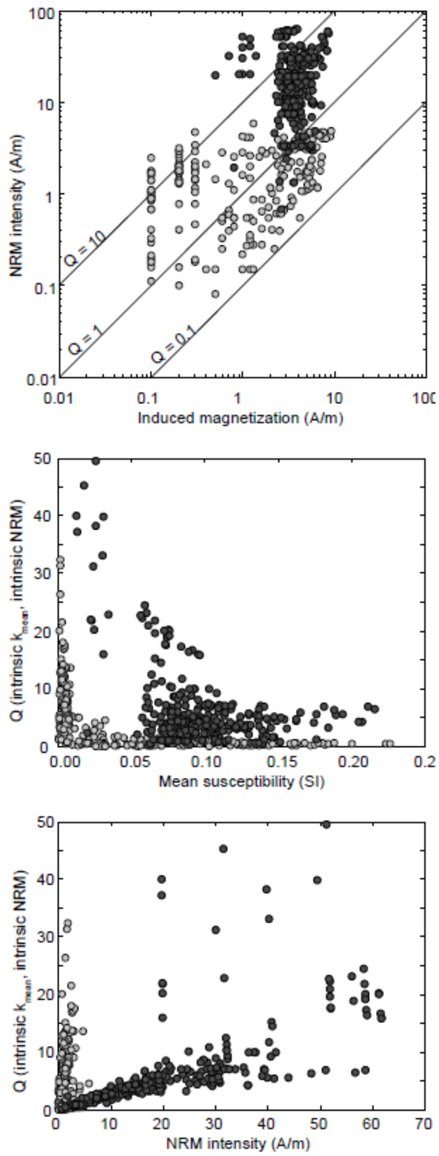

Figure 7: Q-plot, and variation of Q with mean susceptibility or NRM (light grey: samples throughout intrusion, dark grey: MCU IVe' layer).

3.3 Magnetic survey

Geological maps and aeromagnetic data provided by NGU [*Fugro Airborne Surveys*, 2010; *Nasuti et al.*, 2015; *Olesen et al.*, 2015] were used initially to select locations for ground magnetic profiles. Locations and profile orientations were chosen such that these profiles are approximately normal to the trend of the layering and the strong negative anomaly associated with the MCU IVe' layer of the BKS intrusion. This anomaly is best defined and strongest in the east of the intrusion. Ground magnetic profiles were recorded using a Geometrics G859AP Cesium Vapor Magnetometer, taking 5 total field readings per second, and simultaneous GPS recording. Most profiles were measured in two directions (forward and backwards) to increase signal quality and assess reproducibility. Profiles in the east and northeast were additionally linked by one set of profiles ca. parallel to the trend of the anomaly. Before the ground magnetic data was converted to straight profiles, spikes due to e.g. power lines were removed from each measured line using a median filter. All measurement points were then projected onto the profile by assuming a 2D structure extending infinitely normal to the profile. 500 segments of equal length were defined along each profile, and a weighted average taken of all points within the segment, with weighting factors equal to the inverse square of the distance to the profile, so that the measurement points closer to the projected line have a stronger influence than those further away. Ground magnetic profiles generally confirm previously published results from aeromagnetic and ground magnetic data [*McEnroe et al.*, 2004a; *McEnroe et al.*, 2004b]. The ground magnetic data show greater variations at smaller scale.

3.4 Potential field modeling

Figure 8 shows the expected contributions of isotropic and anisotropic induced, as well as remanent anomalies (forward models) and projected ground magnetic data. The intention of this study is to characterize how much each of these components would contribute to an anomaly, and how strong the effect of anisotropy would be, and not creating a detailed model of the subsurface. The ground magnetic data is shown for comparison, yet we did not aim to fit these data. Instead, forward models were calculated to quantify the contribution of 1) induced magnetization, 2) anisotropic induced magnetization, 3) remanent magnetization, and 4) resultant magnetization, i.e. the isotropic or the anisotropic induced magnetization plus the remanent magnetization, to the total field anomaly for each profile. The resultant magnetization was obtained by vector addition. Magnetic properties of the source rocks were approximated by the magnetic susceptibility and remanence of surface samples, averaged over several sites along the profile and within the MCU IVe’ layer (Table S2, Supplementary Information). The rocks adjacent to the MCU IVe’ layer have a significantly smaller remanence [*McEnroe et al.*, 2004a; 2009; *McEnroe et al.*, 2001]. For simplicity, and because an accurate representation of the magnetic properties of the adjacent rocks is not necessary for the purpose of this study, their magnetizations were set to zero in all models.

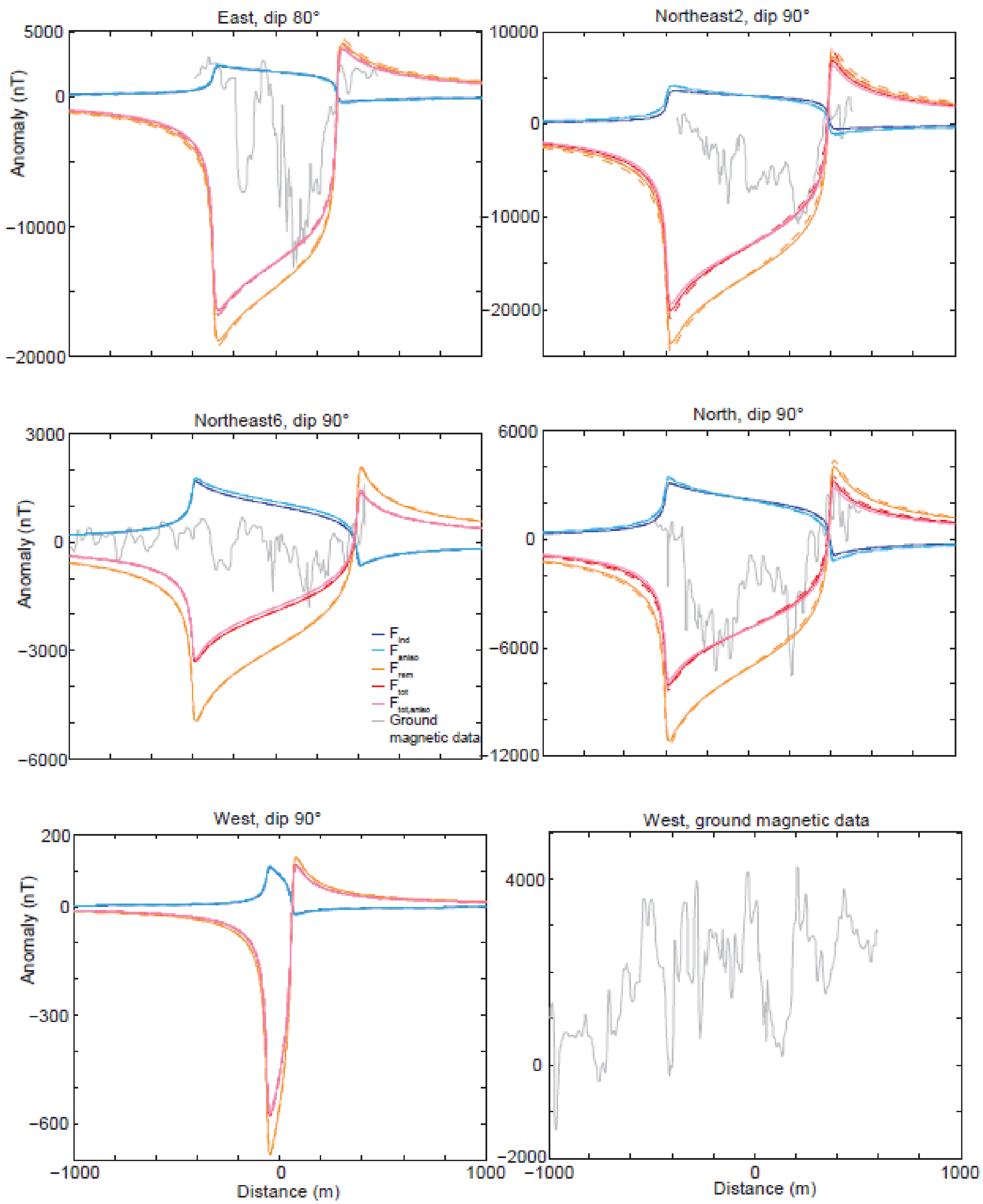

Figure 8: Expected anomalies and ground magnetic profiles. Forward models include isotropic induced anomaly (F_{ind}), anisotropic induced anomaly (F_{aniso}), remanent anomaly (F_{rem}), total anomalies both in the isotropic (F_{tot}) and anisotropic ($F_{tot,aniso}$) case. All models are shown before (dashed) and after (solid) correcting for self-demagnetization effects. Projected ground magnetic data shown for comparison. Note the different intensities for model and data in the West profile.

4. Discussion

4.1 Effects of anisotropy on magnetization and total field anomalies

To date, only few total field anomaly studies have taken anisotropy into account. However, results presented by *Clark and Schmidt* [1994], and the new synthetic models of this study show that anisotropy has significant effects both on the intensity and shape of total field anomalies. Consequently, both interpreted susceptibility as well as interpreted dip can be erroneous if anisotropy is neglected. This will have important consequences for the interpretation of structural features from aeromagnetic maps, or for mining and exploration, where relatively small source bodies have to be hit by drill holes. For example, if the source body is a thick dipping sheet possessing an oblate magnetic fabric with k_3 normal to the sheet, and *P* equals 1.5, the error in interpreted dip can be up to 12°, and the error in estimated susceptibility up to ca. +20/-30%. *Clark and Schmidt* [1994] studied magnetic anomalies over banded iron formations, and state that neglecting anisotropy will lead to serious errors in interpreted dips, and that the error in interpreted dip depends on the angle between inducing field and bedding plane (i.e., k_1-k_2-plane). In their example, *P* equals 2.5 and $\vec{M}_{ind}$ is deflected towards the bedding plane up to 25° when $\vec{H}$ is at an angle of 50° to 60° to the bedding plane. The current study is in agreement with this result, and additionally shows how the intensity and direction of $\vec{M}_{ind}$, and the amplitude and shape of corresponding anomalies, are affected by magnetic fabrics for various combinations of field inclinations and dips of the structure. The deflection of $\vec{M}_{ind}$ varies with the angle between $\vec{H}$ and the bedding or sheet plane, i.e. orientation of magnetic fabric, as reported here and by *Clark and Schmidt* [1994]. If θ denotes the angle between (1) the intersection of the plane of the sheet with a plane normal to strike, and (2) the projection of the field vector to the plane normal to strike, then the deflection of $\vec{M}_{ind}$ is described by $\Delta\theta = \theta - \arctan\left(\frac{\tan\theta}{P}\right)$ (David Clark, pers. comm.). This deflection angle, $\Delta\theta$, corresponds to the error in interpreted dip when an anisotropic sheet is erroneously modeled by an isotropic structure with $\vec{M}_{ind}$ parallel to the inducing field, and increases with increasing degree of anisotropy (Figure 9). The maximum deflection, $\Delta\theta_{Max}$, is observed at different orientations of the magnetic fabric and sheet with respect to $\vec{H}$ for different values of *P*. This maximum possible deflection, $\Delta\theta_{Max} = \arctan\left(\frac{P-1}{2\sqrt{P}}\right)$, occurs for an angle θ of $\theta_{Max} = \arctan\left(\sqrt{P}\right)$ (David Clark, pers. comm.). Overall, the effects of anisotropy on the magnetization vector and on total field anomalies will be weaker for lower *P*-values, and more pronounced for higher degrees of anisotropy, and the maximum effect occurs for different geometries depending on *P*.

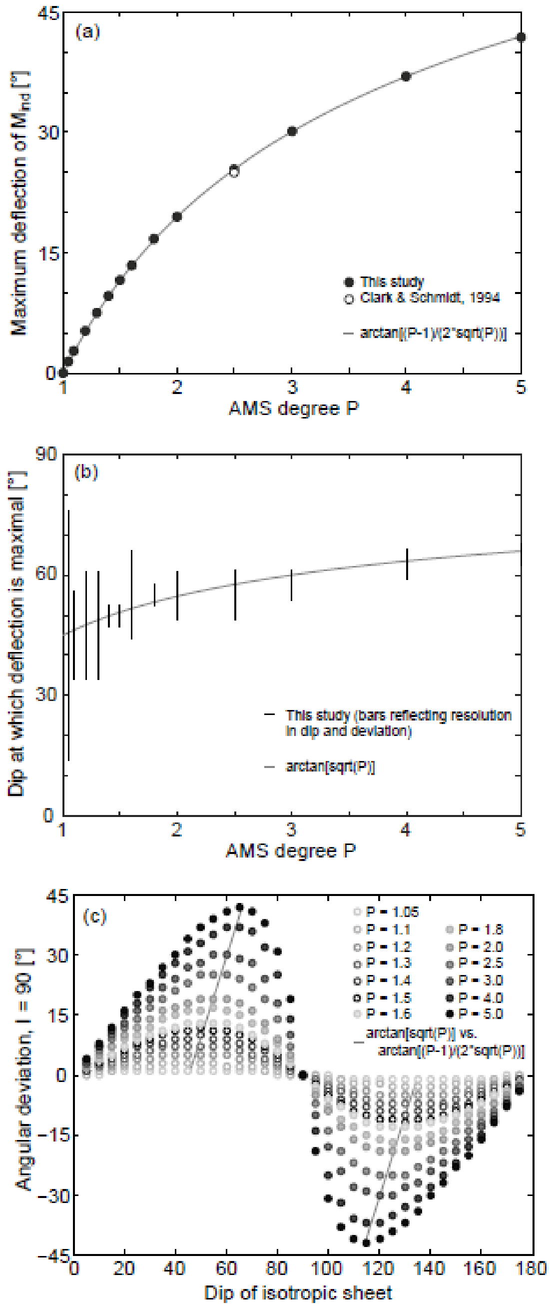

Figure 9: Maximum deflection of magnetization for different P-values (top), the angle between the sheet and inducing field vector projected on a plane normal to strike for which maximum deflection occurs (middle), and the angular difference in dip between isotropic and anisotropic source bodies resulting in the same anomaly shape for different P-values (bottom).

4.2 BKS case study

The amplitude of the negative anomaly (below background) associated with the MCU IVe' layer of the BKS intrusion varies from Heskestad, where it is most prominent, along the layer towards the north and west of the intrusion, where it is still a negative anomaly, but with lower amplitude [*McEnroe et al.*, 2001; *McEnroe et al.*, 2004b]. Generally, many factors can influence the strength of an anomaly, such as geometry (i.e. thickness, dip and trend of the layer, whether it is outcropping at the surface or buried beneath other rocks), mineralogy (i.e. concentration of remanence- and susceptibility-bearing minerals), and changes in magnetic properties within the layer. However, these were taken into account by *McEnroe et al.* [2004b], who used geometry, layer thickness, and mineralogy in their models near Heskestad. To date, the mineralogical origin of the strong magnetization at Heskestad is not fully understood. An additional explanation that has been put forward is the preferred orientation of hemo-ilmenite, i.e. anisotropy [*McEnroe et al.*, 2004b].

Magnetic forward models show that anisotropy influences the part of the anomaly induced by the Earth's field. The difference between anomaly amplitudes over an isotropic or anisotropic body of the same geometry and k_{mean} is up to 1090 nT (27 % of the amplitude for the induced isotropic anomaly; profile Northeast2, cf. Figure 8). Also the shape of the induced anomaly is different for an anisotropic source than for an isotropic source. As shown in the purely synthetic models, using the simplified magnetic fabric (P = 1.5, U = 1, k_3 normal to the layer), and nearly vertical dips as described by *Paludan et al.* [1994], the angular difference between isotropic and anisotropic sheets creating the same induced anomaly shape varies between 0 and ca. 10°, depending on both the profile orientation and the exact dip of the structure. Unlike in the synthetic models, for the forward models the orientation of the magnetic fabric is defined by the susceptibility measurements (cf Table S2), and does not vary with dip of the sheet. Therefore, they do not reproduce the dip-dependence seen in the synthetic models. They do, however display a similar dependence on profile orientation. In this case, the angular difference depends on the profile orientation and magnetic susceptibility tensor, and is 3° (north profile), -1° (west profile), -2° (east profile), -7° (northeast6 profile), or -9° (northeast2 profile). The profile modeled by *McEnroe et al.*, [2004b] is oriented approximately E-W in the east of the intrusion (Heskestad area) and estimated dips were ca. 80° for the contacts between layers of the intrusion. The field inclination is ca. 70°, however, only the vertical component contributes to anomalies for profiles normal to the declination. In this case, the expected change in interpreted dip for the induced anomaly when anisotropy is taken into account would be 5° (cf. Figure 4).

The total observed anomaly is a superposition of the induced and remanent components of the anomaly. Depending on whether induced and remanent magnetization point in similar or opposite directions, the effects of anisotropy would increase or decrease the total anomaly. The effect of (induced) anisotropy on the total anomaly also depends on the relative importance of induced and remanent components. Figure 8 shows that the anomalies are remanence-dominated. Therefore, the induced magnetization, and the effects of anisotropy thereupon, are minimal, particularly in the eastern part of MCU IVe', and anisotropy has mainly an indirect effect, via the NRM direction. *Biedermann et al.* [2017] found that the NRM directions in IVe' are tilted away from the paleofield and towards maximum susceptibility, and most anisotropy corrections lead to a 2–12° change in the NRM direction. These effects are taken into account when the NRM direction used for modeling is determined based on magnetization measurements on samples along the profile rather than an average direction for the entire area of the intrusion. One challenge that arises from the fact that the remanent and total magnetizations over the MCU IVe' are so intense, especially close to Heskestad, is that the local field is disturbed and both its intensity and direction are affected by the secondary field that is produced by the remanent magnetization. Therefore, more work will be needed to include this deflection of the inducing field to the anomaly models, if the goal of a study is to model the detailed geometry and properties of the source body, rather than to investigate contributions from different sources as has been done in the present work. As a consequence of this field deflection, also compass-based sample orientations have to be corrected for, either by using a sun compass or by measuring the direction towards a known far-away point on the map.

4.3 Other settings

The results of the present study can be applied to other geological settings where a planar structural feature possesses magnetic anisotropy with the minimum susceptibility normal to the plane, and a similar *P*-value as the rocks of the BKS. This may be relevant for other mafic layered intrusions, or layered intrusions in general, dikes, banded iron formations, fault and shear zones, or strongly foliated metamorphic and igneous rocks. Several examples will be given here; however, note that reported P-values have not necessarily been measured in a field similar to the geomagnetic field, so that field-dependence may play a role.

Not all layered intrusions have equally strong magnetic fabrics as the cumulate series of the BKS. For example, previously reported *P*-values for the Bushveld Complex, South Africa, range up to 1.4, but are mostly around 1.1 [*Feinberg et al.*, 2006; *Ferré et al.*, 1999]; for the Insizwa layered mafic sill, Karoo Igneous Province, South Africa P_j-values range up to 1.3, but are mainly below 1.2, and *P* often less than 1.1 [*Ferré et al.*, 2002; *Maes et al.*, 2008]. Also for the Rum Eastern Layered Series, NW Scotland, mainly *P'* less than 1.1 have been reported [*O'Driscoll et al.*, 2007]. On the other hand, *Selkin et al.* [2000] describe strong anisotropy of anhysteretic and thermal remanence with *P* ~2.5 in anorthosite samples from the Archean Stillwater Complex, Montana, USA. *Bolle et al.* [2000] investigated magnetic fabrics in the charnockitic igneous rocks of the BKS, and found *P'* up to 2.1, and with k_3 normal to the layering/foliation. Magnetic anisotropy in jotunitic dikes in the Rogaland Anorthosite Province, SW Norway, possess P_j up to ~1.4, and the magnetic foliation is believed to be parallel to the mean dike planes [*Bolle et al.*, 2010].

Schmidt et al. [2007] give an overview of susceptibilitites parallel and normal to bedding in banded iron formations (BIFs): the susceptibility is smallest normal to the bedding plane, and *P*-values are between 1.4 and 2.5 for eight locations, and ≤ 1.1 in four formations. Thus, most BIFs exhibit larger mean P-values than what was used for the synthetic models presented here, and the effect of the anisotropy will be even stronger, leading e.g. to a larger error in interpreted dip of the structure when anisotropy is neglected. On the importance of magnetic anisotropy in BIFs, *Clark and Schmidt* [1994] state that Q values of BIFs depend on the orientation of the bedding plane with respect to the geomagnetic field.

Strong magnetic fabrics with the minimum susceptibility normal to macroscopic foliation or structure have also been reported in fault and shear zones. *Housen et al.* [1995] found *P* up to 2.06 in mylonite and ultra-mylonite samples from the Parry Sound shear zone, Ontario Grenville Province, Canada. The Storsjön-Edsbyn deformation zone, central Sweden, exhibits *P* up to 3.1 [*Mattsson and Elming*, 2001], and *P'* up to 4.8 have been measured in samples from the Slipsiken shear zone in the Scandinavian Caledonides [*Kontny et al.*, 2012]. *Bascou et al.* [2002] investigated mylonitic granulites in the high-temperature Padua shear zone, Ribeira Belt, SE Brazil, and found site-mean *P*-values up to 5.5.

The results presented here can also be adapted to source bodies of different shapes, and have implications for exploration geophysics, e.g. the search for ore bodies. Strong anisotropy has been described in hemo-ilmenite ore deposits at Allard Lake, Canada (*P* up to 3.7 [*Hargraves*, 1959], and Pj up to 4.3 [*Bolle et al.*, 2014]) and in pyrrhotite ore (*P* ~1.7) [*Schwarz*, 1974, cited in *Hrouda*, 1980]. Also buried ore bodies may display magnetic anisotropy. Exploration studies could in this case miss the target when the location for drilling was chosen based on purely isotropic models.

5. Conclusions

Magnetic fabrics in rocks affect the direction and intensity of induced and/or remanent magnetization. This in turn leads to different shapes and amplitudes of total magnetic field anomalies as compared to the anomalies generated by an isotropic body of the same geometry. Therefore, and because any potential field anomalies can be modeled by several combinations of source geometry and magnetic properties of the body, neglecting magnetic anisotropy may result in errors of interpreted dip or susceptibility of the source. The figures in this paper can be used as a reference to estimate the effect of anisotropy on magnetization and total field anomalies for various combinations of source geometry, profile orientation, field direction, and degree of anisotropy. Thus, they can help estimate errors in interpreted dip for future surveys.

In the BKS case study, whereas the source of the anomaly is not entirely understood, AMS does affect the induced magnetization and its contribution to the anomaly. However, the measured anomalies correlated with IVe' are dominated by remanent magnetization, which is deflected towards the maximum susceptibility direction. Hence, in the BKS IVe' layer, anisotropy mainly affects the anomalies via the NRM directions.

Effects of magnetic anisotropy on total field anomalies should be considered for source bodies with strong anisotropy, e.g. layered intrusions, BIFs or shear zones. The results presented in this study provide a first estimate of errors that will occur when anisotropy is not taken into account during modeling of magnetic anomalies of these structures.

Acknowledgments

Peter Robinson, Norwegian Geological Survey (NGU), helped planning the fieldwork, and provided very thorough valuable comments on the manuscript. We are grateful to Alexander Michels, NTNU, for help with fieldwork, and to Bjarne SG Almqvist, Uppsala University, and Morgan Ganerød, NGU, for access to their instruments. Christine Fichler, NTNU, is thanked for helpful discussions about forward modeling of the ground magnetic data. The aeromagnetic map shown in Figure 5 comes from digital aeromagnetic data from the Coop project (Crustal Onshore-Offshore Project) of the Geological Survey of Norway. We are grateful to David Clark and Fatima Martin-Hernandez whose thoughtful reviews helped to improve the manuscript. This study was funded by Swiss National Science Foundation project P2EZP2-155517 to AR Biedermann, NTNU and Research Council of Norway project 222666 to SA McEnroe. Data can be found in the Supporting Information.

References

Arkani-Hamed, J., and G. Celetti (1989), Effects of thermal remanent magnetization on the magnetic anomalies of intrusives, *Journal of Geophysical Research*, *94*(86), 7364-7378.

Bascou, J., M. I. B. Raposo, A. Vauchez, and M. Egydio-Silva (2002), Titanohematite lattice-preferred orientation and magnetic anisotropy in high-temperature mylonites, *Earth and Planetary Science Letters*, *198*, 77-92.

Biedermann, A. R., F. Heidelbach, M. Jackson, D. Bilardello, and S. A. McEnroe (2016), Magnetic fabrics in the Bjerkreim Sokndal Layered Intrusion, Rogaland, Southern Norway: Mineral Sources and Geological Significance, *Tectonophysics*, *in review*.

Biedermann, A. R., M. Jackson, D. Bilardello, and S. A. McEnroe (2017), Effect of magnetic anisotropy on the natural remanent magnetization in the MCU IVe' layer of the Bjerkreim Sokndal Layered Intrusion, Rogaland, Southern Norway, *Journal of Geophysical Research – Solid Earth*.

Blakely, R. J. (1996), *Potential Theory in Gravity and Magnetics Applications*, Cambridge University Press, Cambridge, UK.

Bolle, O., M. Besse, and H. Diot (2010), Magma flow and feeder chamber location inferred from magnetic fabrics in jotunitic dykes (Rogaland anorthosite province, SW Norway), *Tectonophysics*, *493*(1-2), 42-57, doi:10.1016/j.tecto.2010.06.017.

Bolle, O., B. Charlier, J. Bascou, H. Diot, and S. A. McEnroe (2014), Anisotropy of magnetic susceptibility versus lattice- and shape-preferred orientation in the Lac Tio hemo-ilmenite ore body (Grenville province, Quebec), *Tectonophysics*, *629*, 87-108.

Bolle, O., H. Diot, and J.-C. Duchesne (2000), Magnetic fabric and deformation in charnockitic igneous rocks of the Bjerkreim-Sokndal layered intrusion (Rogaland, Southwest Norway), *Journal of Structural Geology*, *22*, 647-667.

Bolle, O., R. I. F. Trindade, J. L. Bouchez, and J. C. Duchesne (2002), Imaging downward granitic magma transport in the Rogaland Igneous Complex, SW Norway, *Terra Nova*, *14*, 87-92.

Brown, L. L., and S. A. McEnroe (2015), 916 Ma Pole for southwestern Baltica: palaeomagnetism of the Bjerkreim-Sokndal layered intrusion, Rogaland Igneous Complex, southern Norway, *Geophysical Journal International*, *203*(1), 567-587, doi:10.1093/gji/ggv299.

Chen, D.-X., J. A. Brug, and R. B. Goldfarb (1991), Demagnetizing factors for cylinders, *IEEE Transactions on Magnetics*, *27*(4), 3601-3619.

Clark, D. A. (1997), Magnetic petrophysics and magnetic petrology: aids to geological interpretation of magnetic surveys, *Journal of Australian Geology and Geophysics*, *17*, 83-103.

Clark, D. A. (2014), Methods for determining remanent and total magnetizations of magnetic sources - a review, *Exploration Geophysics*, *45*, 271-304.

Clark, D. A., and D. W. Emerson (1999), Self-Demagnetisation, *Preview*, *79*, 22-25.

Clark, D. A., and P. W. Schmidt (1994), Magnetic properties and magnetic signatures of BIFs of the Hamersley Basin and Yilgarn Block, Western Australia, *In: Geophysical Signatures of Western*

Australian Mineral Deposits, Geology and Geophysics Department (Key Centre) & UWA Extension, University of Western Australia, *26*, 343-354.

Deemer, S., and C. Hurich (1997), Seismic image of the basal portion of the Bjerkreim-Sokndal layered intrusion, *Geology*, *25*(12), 1107-1110.

Duchesne, J. C. (2001), The Rogaland Intrusive Massifs - an excursion guide, *NGU Report*, *2001.029*, 139 pp.

Duchesne, J. C., and B. Charlier (2005), Geochemistry of cumulates from the Bjerkreim–Sokndal layered intrusion (S. Norway). Part I: Constraints from major elements on the mechanism of cumulate formation and on the jotunite liquid line of descent, *Lithos*, *83*(3-4), 229-254, doi:10.1016/j.lithos.2005.03.004.

Emerson, D. W., D. A. Clark, and S. J. Saul (1985), Magnetic exploration models incorporating remanence, demagnetization and anisotropy: HP 41C handheld computer algorithms, *Exploration Geophysics*, *16*, 1-122.

Feinberg, J. M., H.-R. Wenk, G. R. Scott, and P. R. Renne (2006), Preferred orientation and anisotropy of seismic and magnetic properties in gabbronorites from the Bushveld layered intrusion, *Tectonophysics*, *420*(3-4), 345-356, doi:10.1016/j.tecto.2006.03.017.

Ferré, E. C., C. Bordarier, and J. S. Marsh (2002), Magma flow inferred from AMS fabrics in a layered mafic sill, Insizwa, South Africa, *Tectonophysics*, *354*, 1-23.

Ferré, E. C., J. Wilson, and G. Gleizes (1999), Magnetic susceptibility and AMS of the Bushveld alkaline granites, South Africa, *Tectonophysics*, *307*, 113-133.

Florio, G., M. Fedi, A. Rapolla, D. M. Fountain, and P. N. Shive (1993), Anisotropic magnetic susceptibility in the continental crust and its implications for the shape of magnetic anomalies, *Geophysical Research Letters*, *20*(23), 2623-2626.

Fugro Airborne Surveys (2010), Processing Report, Fixed-wing airborne magnetic and radiometric survey over the Bergen-Stavanger Region (BESTAS-10), NORWAY.Report FCR 2516, 55 pp.

Guerrero-Suarez, S., and F. Martin-Hernandez (2012), Magnetic anisotropy of hematite natural crystals: increasing low-field strength experiments, *International Journal of Earth Science (Geologische Rundschau)*, 101, 625-636.

Guo, W., M. C. Dentith, R. T. Bird, and D. A. Clark (2001), Systematic error analysis of demagnetization and implications for magnetic interpretation, *Geophysics*, *66*(2), 562-570.

Hall, D. H. (1959), Direction of polarization determined from magnetic anomalies, *Journal of Geophysical Research*, *64*(11), 1945-1959.

Hargraves, R. B. (1959), Magnetic anisotropy and remanent magnetism in hemo-ilmenite from ore deposits at Allard Lake, Quebec, *Journal of Geophysical Research*, *64*(10), 1565-1578, doi:10.1029/JZ064i010p01565.

Housen, B. A., B. A. van der Pluijm, and E. J. Essene (1995), Plastic behavior of magnetite and high strains obtained from magnetic fabrics in the Parry Sound shear zone, Ontario Grenville Province, *Journal of Structural Geology*, *17*(2), 265-278.

Hrouda, F. (1980), Magnetocrystalline anisotropy of rocks and massive ores: a mathematical model study and its fabric implications, *Journal of Structural Geology*, *2*(4), 459-462.

Hrouda, F. (1982), Magnetic anisotropy of rocks and its application in geology and geophysics, *Geophysical Surveys*, *5*, 37-82.

Jelinek, V. (1981), Characterization of the magnetic fabric of rocks, *Tectonophysics*, *79*, T63-T67.

Kontny, A., R. Engelmann, J. C. Grimmer, R. O. Greiling, and A. Hirt (2012), Magnetic fabric development in a highly anisotropic magnetite-bearing ductile shear zone (Seve Nappe Complex, Scandinavian Caledonides), *International Journal of Earth Sciences (Geologische Rundschau)*, *101*, 671-692.

Maes, S. M., E. C. Ferré, B. Tikoff, P. E. Brown, and J. S. Marsh (2008), Rock magnetic stratigraphy of a mafic layered sill: A key to the Karoo volcanics plumbing system, *Journal of Volcanology and Geothermal Research*, *172*, 75-92.

Mattsson, H., and S. Å. Elming (2001), Magnetic fabrics and paleomagnetism of the Storsjön-Edsbyn deformation zone, central Sweden, *Precambrian Research*, *107*, 265-281.

Martin-Hernandez, F., M.J. Dekkers, I.M.A. Bominaar-Silkens, and J.C. Maan (2008), Magnetic anisotropy behaviour of pyrrhotite as determined by low- and high-field experiments. *Geophysical Journal International*, doi: 10.1111/j.1365-246X.2008.03793.x

McEnroe, S. A., L. L. Brown, and P. Robinson (2004a), Earth analog for Martian magnetic anomalies: remanence properties of hemo-ilmenite norites in the Bjerkreim-Sokndal intrusion, Rogaland, Norway, *Journal of Applied Geophysics*, *56*(3), 195-212, doi:10.1016/j.jappgeo.2004.07.002.

McEnroe, S. A., L. L. Brown, and P. Robinson (2009), Remanent and induced magnetic anomalies over a layered intrusion: Effects from crystal fractionation and magma recharge, *Tectonophysics*, *478*(1-2), 119-134, doi:10.1016/j.tecto.2008.11.021.

McEnroe, S. A., P. Robinson, and P. T. Panish (2001), Aeromagnetic anomalies, magnetic petrology, and rock magnetism of hemo-ilmenite- and magnetite-rich cumulate rocks from the Sokndal Region, South Rogaland, Norway, *American Mineralogist*, *86*, 1447-1468.

McEnroe, S. A., J. R. Skilbrei, P. Robinson, F. Heidelbach, F. Langenhorst, and L. L. Brown (2004b), Magnetic anomalies, layered intrusions and Mars, *Geophysical Research Letters*, *31*(19), doi:10.1029/2004gl020640.

Nasuti, A., O. Olesen, V. Barnawal, and M.-A. Dumais (2015), Compilation of aeromagnetic data. In: Olesen et al. (eds.) Coop Phase 2 Crustal Onshore-Offshore Project. NGU Report 2015.063. 11-24.

O'Driscoll, B., R. B. Hargraves, C. H. Erneleus, V. Troll, C. H. Donaldson, and R. J. Reavy (2007), Magmatic lineations inferred from anisotropy of magnetic susceptibility fabrics in units 8, 9, and 10 of the Rum Eastern Layered Series, NW Scotland, *Lithos*, *98*(1-4), 27-44, doi:10.1016/j.lithos.2007.01.009.

Olesen, O., V. Barnawal, M. Brönner, E. Dalsegg, M.-A. Dumais, J. Gellein, L. Gernigon, T. Heldal, B.E. Larsen, T. Lauritsen, O. Lutro, Y. Maystrenko, A. Nasuti, D. Roberts, H. Rueslåtten, J.S. Rønning, T. Slagstad, A. Solli, and A. Stampolidis (2015), Coop Phase 2 Crustal Onshore-Offshore Project. NGU Report 2015.063. 410 pp.

Osborn, J. A. (1945), Demagnetizing factors of the general ellipsoid, *Physical Review 67*(11-12), 351-357.

Paludan, J., U. B. Hansen, and N. Ø. Olesen (1994), Structural evolution of the Precambrian Bjerkreim-Sokndal intrusion, South Norway, *Norsk Geologisk Tidsskrift*, *74*, 185-198.

Porath, H., F. D. Stacey, and S. Cheam (1966), The choice of specimen shape for magnetic anisotropy measurements on rocks *Earth and Planetary Science Letters*, *1*, 92.

Robins, B., and J. R. Wilson (2001), The Bjerkreim-Sokndal layered intrusion, in *The Rogaland Intrusive Massifs - an excursion guide*, edited by J. C. Duchesne, NGU Report, Trondheim, Norway.

Robinson, P., K. Fabian, S. A. McEnroe, and F. Heidelbach (2013), Influence of lattice-preferred orientation with respect to magnetizing field on intensity of remanent magnetization in polycrystalline hemo-ilmenite, *Geophysical Journal International*, *192*(2), 514-536, doi:10.1093/gji/ggs046.

Sato, M., and Y. Ishii (1989), Simple and approximate expressions of demagnetizing factors of uniformly magnetized rectangular rod and cylinder, *Journal of Applied Physics*, *66*(2), 983-985.

Schmidt, P. W., S. A. McEnroe, D. A. Clark, and P. Robinson (2007), Magnetic properties and potential field modeling of the Peculiar Knob metamorphosed iron formation, South Australia: An analog for the source of the intense Martian magnetic anomalies?, *Journal of Geophysical Research*, *112*(B3), doi:10.1029/2006jb004495.

Selkin, P. A., J. S. Gee, L. Tauxe, W. P. Meurer, and A. J. Newell (2000), The effect of remanence anisotropy on paleointensity estimates: a case study from the Archean Stillwater Complex, *Earth and Planetary Science Letters*, *183*, 403-416.

Smellie, D. W. (1956), Elementary approximation in aeromagnetic interpretation, *Geophysics*, *21*(4), 1021-1040.

Smithson, S. B., and I. B. Ramberg (1979), Gravity interpretation of the Egersund anorthosite complex, Norway: Its petrological and geothermal significance, *Geological Society of America Bulletin, Part 1*, *90*, 199-204.

Sutton, D. J., and W. G. Mumme (1957), The effect of remanent magnetization on aeromagnetic interpretation, *Australian Journal of Physics*, *10*(4), 547-557.

Wilson, J. R., B. Robins, F. M. Nielsen, J. C. Duchesne, and J. Vander Auwera (1996), The Bjerkreim-Sokndal layered intrusion, Southwest Norway, in *Layered Intrusions*, edited by R. G. Cawthorn, pp. 231-255, Elsevier, Amsterdam.

Worm, H.-U. (1991), Multidomain susceptibility and anomalously strong low field dependence of induced magnetization in pyrrhotite. *Physics of the Earth and Planetary Interiors*, 69(1-2), 112-118.

Worm, H.-U., D. Clark, and M.J. Dekkers (1993), Magnetic susceptibility of pyrrhotite: grain size, field and frequency dependence. *Geophysical Journal International,* 114(1), 127-137.

Zietz, I., and R. G. Henderson (1956), A preliminary report on model studies of magnetic anomalies of three-dimensional bodies, *Geophysics*, *21*(3), 794-814.